Available online at www.sciencedirect.com

SciVerse ScienceDirect

Ceramics International 39 (2013) 4899–4906

CERAMICS INTERNATIONAL

www.elsevier.com/locate/ceramint

Study on stability and electrical performance of yttrium and bismuth co-doped $BaCeO_3$

Xiaowei Chi, Jingchao Zhang, Meifen Wu, Yu Liu, Zhaoyin Wen*

CAS Key Laboratory of Materials for Energy Conversion, Shanghai Institute of Ceramics, Chinese Academy of Sciences, 1295 DingXi Road, Shanghai 200050, PR. China

Received 27 September 2012; received in revised form 12 November 2012; accepted 26 November 2012
Available online 3 December 2012

Abstract

Yttrium and bismuth co-doped $BaCeO_3$ ($BaCe_{0.8-x}Y_{0.2}Bi_xO_{3-\delta}$, $x=0$, 0.1, 0.3, 0.5, abbreviated as B0, B10, B30, B50, respectively) powders were successfully synthesized by the citrate–EDTA auto-ignition method and dense ceramics were also obtained. The investigations were mainly focused on the chemical stability and electrical performance of the bismuth doped $BaCe_{0.8}Y_{0.2}O_{3-\delta}$. The phase and thermal analysis of the powders demonstrated that the appropriate amount of Bi dopant can well stabilize $BaCeO_3$ (e.g. Bi=0.3 and 0.5) and prevented them from boiling water damage, whilst the stability in CO_2-containing atmosphere degraded with the increase of the bismuth content. It was demonstrated that in wet air, the conductivities of B30 and B50 reached as high as 0.20 S/cm and 0.71 S/cm at 700 °C, respectively. And both were one order of magnitude higher than that of B0. An electron conduction mechanism for the bismuth doped $BaCeO_3$ specimen was proposed. Yttrium and bismuth co-doping exerted influences on both the chemical stability and electrical performance.

Keywords: A. Sol–gel processes; B. Defects; C. Electrical conductivity; D. Perovskites

1. Introduction

Proton conductor with perovskite structure reported in 1981 by Iwahara et al. [1] has been explored in many applications, such as fuel cells [2], ammonium synthesis [3], hydrogen pumps [4] and so on. In particular, there are many advantages for protonic ceramic fuel cells (SOFC-H^+) over oxygen ionic ceramic fuel cells (SOFC-O^{2-}) [5]. It is unnecessary to circulate the fuel and can work at lower temperatures. Moreover, SOFC-H^+ usually shows better cell performance than that of SOFC-O^{2-}. But its real applications are still limited owing to many problems, especially for the sake of protonic conductive ceramic electrolytes. The instability of the solid electrolytes in the atmosphere containing H_2O and CO_2 and their low electrical conductivity are the most worrying issues. Furthermore, suitable anode and cathode materials with mixed ionic–electronic conduction, low polarization resistance and good stability are also under development.

A typical example of solid electrolytes used in SOFC-H^+ is $BaCe_{0.8}Y_{0.2}O_{3-\delta}$, which has a superior protonic conductivity but lacks chemical stability in CO_2 and H_2O [6]. Kreuer found that the electronegativity of ions in crystal lattice played a key factor that greatly influenced the stability of the system [7]. So up to now the introduction of elemental dopants into the host has been being an attractive way to improve its stability. For example, elements with higher electronegativity (Mulliken Electronegativity) than cerium ($Ce^{4+}=51$ eV), such as zirconium ($Zr^{4+}=57.9$ eV), have been demonstrated as good candidates of dopants to enhance the stability of $BaCeO_3$ by many researchers [8–10]. Among them, bismuth (Bi) is also considered to be a special element even with much higher electronegativity (e.g. $Bi^{5+}=72$ eV) than that of zirconium and therefore be inevitable to influence the stability of the host. Additionally, the fact that Bi ions in $BaBiO_3$ possess two valences: Bi^{3+} and Bi^{5+}, may also exert some effect on the host [11]. Furthermore, it is well known that Bi_2O_3 is an

*Corresponding author. Tel.: +86 21 52411704; fax: +86 21 52413903.
E-mail address: zywen@mail.sic.ac.cn (Z. Wen).

0272-8842/$ - see front matter © 2012 Elsevier Ltd and Techna Group S.r.l. All rights reserved.
http://dx.doi.org/10.1016/j.ceramint.2012.11.083

effective sintering aid of ceramics [12,13]. Therefore, in this work yttrium and bismuth were simultaneously introduced into $BaCeO_3$ lattice in order to investigate the effect of co-doping on the chemical stability, sinterability and electric properties.

2. Experimental

2.1. Sample preparation

At present, researchers widely use the combustion method to prepare homogenous and ultrafine oxide powders, especially the multi-components oxide powders [14–16]. A citrate–ethylenediaminetetraacetate acid (EDTA) auto-ignition method was adopted in this work.

$Ba(NO_3)_2$, $Ce(NO_3)_3 \cdot 6H_2O$, $Y(NO_3)_3 \cdot 6H_2O$ and $Bi(NO_3)_3 \cdot 5H_2O$ (A.R.) in stoichiometric proportion were dissolved in pre-mixed EDTA solution containing ammonium. The resulting solution was adjusted to be neutral by dropping nitric acid solution and stirred for 12 h to form uniform metal ion–EDTA complex compound. Then the citric acid (citric acid: metal nitrates: EDTA molar ratio = 1.5:1:1) was added to the above complex compound and the resulting mixture was kept stirring overnight. Water was slowly evaporated at 80 °C. As soon as the sol formed, it was transferred to an electric oven and heated until auto-ignition happened. The as-burnt powder was heat-treated at 600 °C for 3 h to remove organic residues and further calcined to form final structures at a proper temperature on the basis of the TG–DSC analytical results.

2.2. Characterization techniques

X-ray diffraction (XRD, Rigaku, Ultima IV) with CuKα radiation, was used to characterize the phase change of the powders before and after boiling water treatment. With regard to the stability against CO_2, thermogravimetric analysis of the synthesized powders in $97\%N_2+3\%CO_2$ atmosphere [17,18] at 700 °C for 2 h was carried out on a NETZSCH STA 409PC thermal analyzer.

For the sake of obtaining dense ceramics, dilatometry (Netzsch, DIL 402C) on the green body cylinders (Φ5 mm × 10 mm) was performed in nitrogen in order to determine a proper sintering temperature. Pellets (2.5 mm in thickness, 12 mm in diameter) were iso-statically pressed at 250 MPa and sintered. The microstructures of the sintered pellets were observed on a scanning electron microscope (SEM, HITACHI, S3400N). To characterize the electrical performance, platinum paste was printed on both polished sides of the sintered disks and subsequently calcined at 800 °C for 30 min to obtain porous platinum electrodes. Then the A.C. impedance test was taken to measure the electrical conductivity in wet air and nitrogen from 750 to 500 °C with an interval of 50 °C by using the electrochemical station Autolab PGSTAT302. The atmospheres were humidified by passing them through a water bubbler. A.C. amplitude of 10 mV and frequency range from 1 MHz to 0.01 Hz were applied for the tests.

3. Results and discussion

3.1. Phase formation

Fig. 1 shows the XRD patterns of B0, B10, B30 and B50 powders calcined at 1000 °C, 900 °C, 800 °C and 800 °C, respectively. The appropriate calcination temperatures of each precursor with different contents of bismuth after combustion were firstly determined based on TG-DSC curves. From Fig. 1, no any impurity peaks are found in all the samples, indicating that $BaCeO_3$ and $BaBiO_3$ have well formed a solid solution $Ba(Ce,Bi)O_3$ and crystallized the target oxide. Moreover, introducing bismuth into the lattice promote the phase formation of the host to some degree. Comparing the XRD patterns with the PDF cards and previously reported results about $BaCeO_3$ and $BaBiO_3$, the lattice symmetry is found to be different for the undoped and Bi-doped powders. Shown in Table 1, for B0, it is mainly orthorhombic (O), whilst tetragonal (T) for B10 and cubic (T) for B30 and B50. So the substitution of Ce by Bi can enhance the crystal structure symmetry of $BaCeO_3$. Also, three characteristic peaks are indexed in Fig. 1 at the same time. When the contents of Bi reach up to 30% and 50%, slight peak shifts to higher 2Theta are found. The results illustrate that the substitution of Ce with Bi can induce smaller lattice parameters, which is consistent with the results (shown in Table 1) calculated based on the method of the external standard of silicon. It also further indicated that the radius of bismuth in the lattice is smaller than that of cerium. From the ionic radii in octahedral coordination, radius of Ce^{4+} is 0.87 Å, and Bi^{3+} is 1.03 Å, implying that there must be some Bi^{5+} ions in the lattice which have smaller radius of 0.74 Å. That is to say, both Bi^{3+} and Bi^{5+} ions simultaneously exist in the

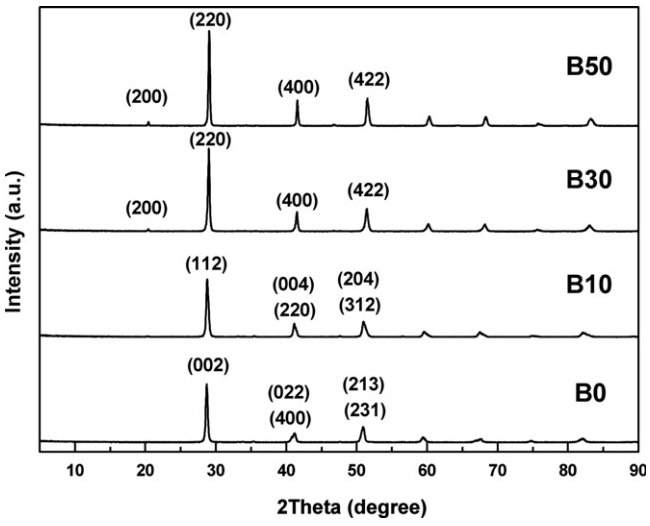

Fig. 1. XRD patterns of calcined powders doped with different contents of Bi.

Table 1
Crystal symmetry and lattice parameters of the $BaCe_{0.8-x}Y_{0.2}Bi_xO_{3-\delta}$ oxides with different contents of Bi.

Bi content	Symmetry	a (Å)	b (Å)	c (Å)	V_c (Å^3)
0	O	8.7958	6.2573	6.2246	342.59
0.1	T	8.7523	6.2556	6.2556	342.50
0.3	C	4.3503	4.3503	4.3503	82.33
0.5	C	4.3399	4.3399	4.3399	81.74

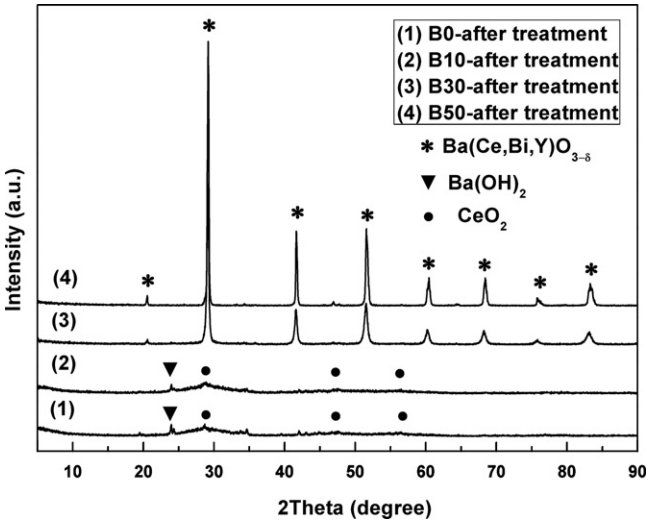

Fig. 2. XRD patterns of powders with different contents of bismuth after the boiling water treatment.

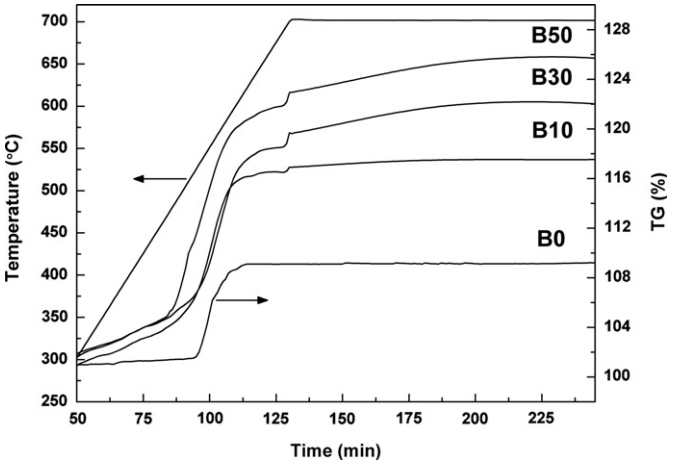

Fig. 3. TGA curves of B0 and bismuth doped powders exposed to 97%N_2+3%CO_2 atmosphere.

$Ba(Ce,Bi)O_3$ lattice. Furthermore, there are more Bi^{5+} ions than Bi^{3+} ions as the average radius of Bi^{3+} and Bi^{5+} ions is larger than that of Ce^{4+} ion. These are in good agreement with the conclusion reported by Drost and Fu [11].

3.2. Stability in H_2O and CO_2 atmospheres

XRD results of B0, B10, B30 and B50 samples after the treatment in boiling water are shown in Fig. 2. It was reported previously that B0 was very unstable and easy to decompose into barium hydroxide and cerium oxide in humid atmospheres [6]. On the contrary, Bi doped samples, especially for the B30 and B50 samples, still retain the original phase structure, demonstrating the significantly enhanced chemical stability of $BaCeO_3$ against water by the Bi dopant. There are two possible reasons for the results. Firstly, the stability of perovskite is associated with the electronegativity of the ions in the lattice. As mentioned before, Bi^{3+} and Bi^{5+} coexist in the samples with the incorporation of Bi, so the electronegativity of Bi is the average, i.e., 53.8 eV. Obviously, it is much higher than that of Ce (51 eV). And, according to Kreuer's conclusion, more acidity will be introduced to the lattice, so the activity of reaction between $BaCeO_3$ and H_2O is significantly weakened [7].

Secondly, the stabilization effect of doped ion on original host can be interpreted from another viewpoint, viz. tolerance factor t. In perovskite, it is defined as

$$t = \frac{r_A + r_O}{\sqrt{2}(r_B + r_O)} \quad (1)$$

According to the XRD results, the average radius of the ions in B-site decreases with the increase of Bi content. As a result, when Bi is introduced into $BaCeO_3$ lattice, the tolerance factor will increase. Bhide and Virkar ever demonstrated that the closer the tolerance factor to unity, the better the stability of perovskite [19]. Consequently, the same conclusion that Bi doped samples exhibit excellent stability against water can be drawn.

Fig. 3 shows the TGA curves of all the powders tested in the atmosphere containing CO_2 (97%N_2+3%CO_2) from 300 °C to 700 °C and held at 700 °C for 2 h. The weight increases of B0, B30 and B50 samples are about 9%, 22% and 26%, respectively. Moreover, the weight increase begins at near 300 °C for B30 and B50, but near 500 °C for B0. The results illustrate that the chemical stability against CO_2 gradually decreases with the increase of Bi content. In order to understand the results, the reactions between $BaCeO_3$ or $BaBiO_3$ and CO_2 are considered as follows:

$$BaCeO_3 + CO_2 \rightarrow BaCO_3 + CeO_2 \quad (2)$$

$$BaBiO_3 + CO_2 \rightarrow BaCO_3 + 1/2Bi_2O_3 + 1/4O_2 \quad (3)$$

Eq. (2) has been demonstrated by many researchers. Here, in order to confirm Eq. (3), the existence of the final reaction product was firstly identified thoroughly. Take B50 as an example; the XRD pattern (depicted in Fig. 4) of the sample after CO_2-containing atmosphere ($97\%N_2+3\%CO_2$) treatment at 700 °C for 2 h evidently shows that the $BaCO_3$, CeO_2 and Bi_2O_3 products formed. Again carefully analyzing the reaction between B50 and CO_2 (Eq. (4)), the theoretical weight increase can be calculated to be 12.7% without the gaseous products. Combining the chemical reaction equilibrium and the practical weight increase of B50 from TG curves (Fig. 3), which is lower than 12.6%, it can be concluded that some oxygen is released during the reaction:

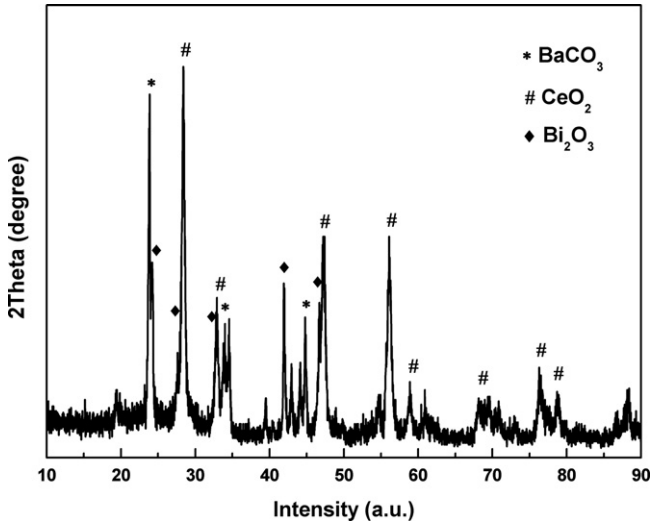

Fig. 4. XRD pattern of B50 powders after treatment under the atmosphere of $97\%N_2+3\%CO_2$ at 700 °C for 2 h.

$$BaCe_{0.3}Bi_{0.5}Y_{0.2}O_{2.9} + CO_2 \rightarrow BaCO_3 + 0.3CeO_2 + 0.25Bi_2O_3 + 0.1Y_2O_3 + 0.125O_2 \quad (4)$$

With respect to the poorer chemical stability against CO_2 when Bi is doped, there are several reasons. First and foremost, it is well known that similar to CeO_2, Bi_2O_3 is insoluble in water but more easily reacts with acids than does CeO_2. Accordingly, Eq. (3) will be accelerated to a great extent due to the reaction between CO_2 and Bi_2O_3. Secondly, different from $BaCeO_3$, the reaction for $BaBiO_3$ relates to oxygen. Then in the atmosphere containing $97\%N_2+3\%CO_2$, of which the oxygen partial pressure is extremely low, the driving force for Eq. (3) is larger than for Eq. (2). Therefore, in terms of the chemical reaction balance, it is suggested that the latter is easier to take place than the former.

Furthermore, it is reasonable to assume that Bi^{5+} in the lattice tends to be reduced into Bi^{3+} in such a low oxygen partial pressure. Then on one hand, the total electronegativity of Bi would become smaller as the electronegativity of Bi^{3+} (35 eV) is smaller than those of Ce^{4+} (51 eV) and Bi^{5+} (72 eV). As a result, the stability was weakened to some extent. On the other hand, the tolerance factor calculated from Eq. (1) is also reduced. The results are ascribed to the increased average ionic radius of Bi when more Bi^{3+} ions are introduced. Consequently, as suggested above, the content of CO_2 in the atmosphere where the materials are used should be well controlled. Considering the instability of B10 against water, it will not be involved in the further studies.

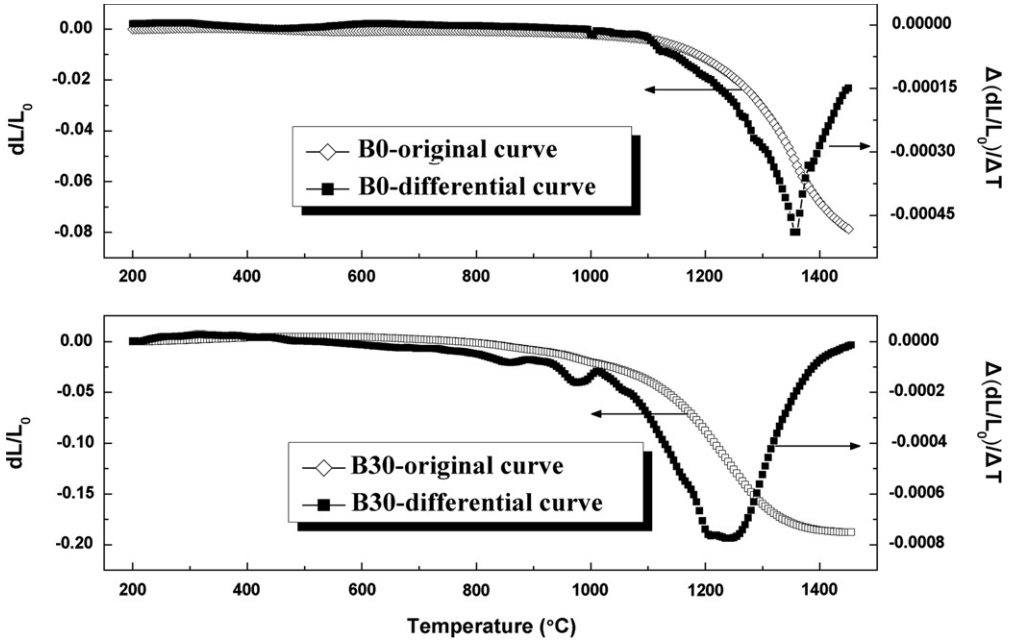

Fig. 5. Linear shrinkage (◇) and differential curves (■) versus sintering temperature of B0 and B30.

3.3. Densification and microstructure

In order to prepare dense ceramic specimens, sinterability of B0 and B30 samples (B50 is similar to B30) was then investigated, as shown in Fig. 5. The linear shrinkage (dL/L_0) for B30 begins at about 900 °C and reaches 18% at 1450 °C, while for B0, its linear shrinkage is only half of that of B30. This result illustrates that B30 has much higher sinterability than that of B0. Bi element doped into $BaCeO_3$ lattice has the same positive effect on the sintering behavior as the promotion effect of Bi_2O_3 compound in the preparation of some other ceramics [12,13]. At the same time, the appropriate sintering temperatures can be acquired from the differential sintering curves. They are ~1380 °C for B0 and as low as 1250 °C for B30. The high sinterability is very favorable for the sample preparation and the corresponding device assemblage.

Fig. 6 shows SEM photographs of the cross section for B0, B30 and B50 pellets sintered at 1400 °C, 1250 °C and 1250 °C for 8 h, respectively. Apparently all the three samples exhibited highly dense morphologies. It can be seen that the microstructure of B0 is significantly different from those of bismuth doped samples. For B0, the grains and grain boundaries are clear; however, they are hard to be distinguished in the B30 and B50 samples. Such features of the doped samples should be beneficial for the transport of conducting species. Generally speaking, the grain boundary resistance dominates the total resistance. Consequently, in principle, the conductivity of B30 and B50 samples, with or without grain boundary contribution, should be larger than that of B0 sample. Detailed results and discussion will be given in the following part.

3.4. Electrical performance

Typical impedance spectra in wet air for B0, B30, B50 and silver (Ag) thread are displayed in Fig. 7. The impedance spectra of the undoped samples differ from those of the Bi-doped samples. For the former (B0), it can be separated into three semicircles, corresponding to bulk, grain boundary and electrodes processes. And the points under zero in $-Z''$ axis are ascribed to the inductance. Nevertheless, for B30, especially for B50, the grain boundary and electrode processes are difficult to detect, which can also be confirmed by the nearly invisible grain boundaries in Fig. 5. And more importantly, the impedance spectrum features of the Bi-doped samples and the silver thread are similar, which firstly indicates that the conduction mechanism of the samples with Bi element may be the same as that of silver. That is to say, the electronic conduction dominates the B30 and B50. Secondly, the influence of the silver electrode thread on the resistance of B30 and B50 sample should be taken into consideration. For accuracy's sake, the four probe dc method was simultaneously used to test the Bi-doped samples. The conductivity σ can be calculated according to the following formula:

$\sigma = l/RS$ where R is the measured resistance, l is the thickness of sample and S is the cross section area of sample.

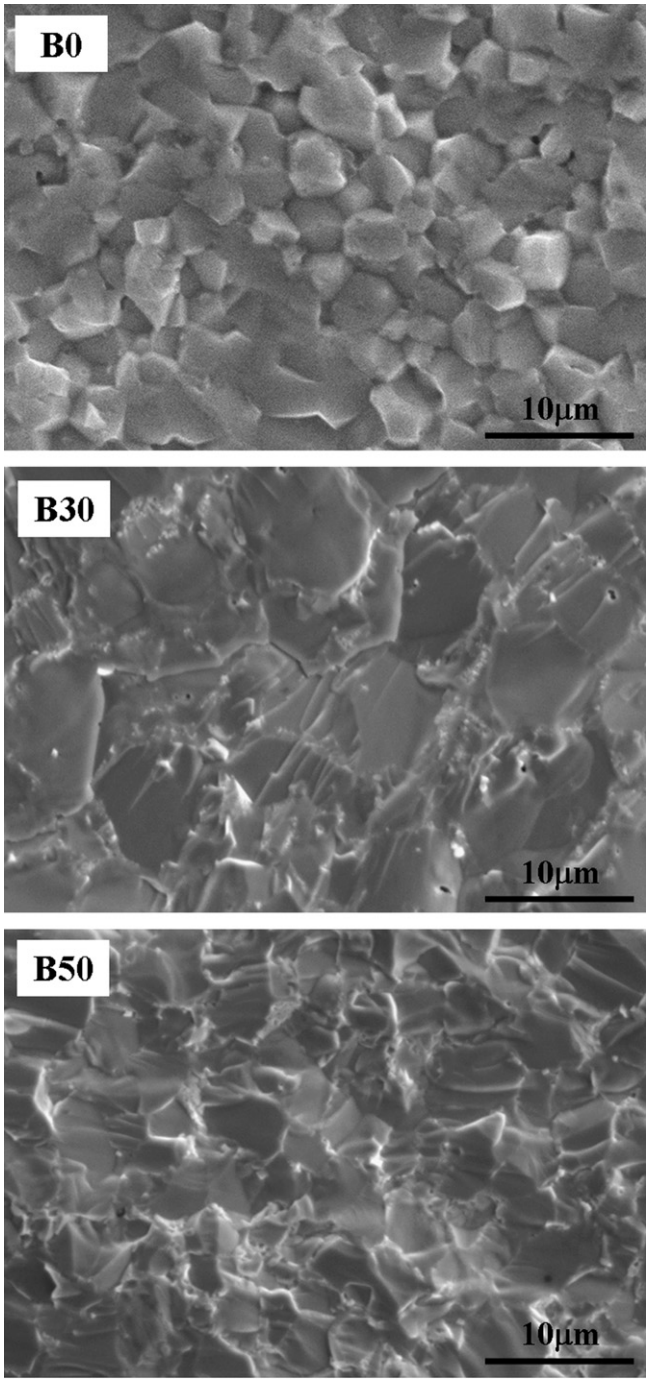

Fig. 6. Microstructure of fractured B0, B30 and B50 sintered pellets.

Arrhenius plots of the total conductivity of B0, B30 and B50 samples were drawn by plotting $\log\sigma$ versus $1000/T$ and are presented in Fig. 8. In wet air (Fig. 7(a)), each of the three samples has an approximately linear relationship between $\log\sigma$ and $1000/T$, illustrating a dominant conducting mechanism for each material.

As is known to all, oxygen vacancies and holes form as the following reactions describe, when acceptor is doped into $BaCeO_3$ [1,20]:

$$Y_2O_3 \overset{CeO_2}{\rightarrow} V_O^{\bullet\bullet} + 2Y'_{Ce} + 3O_O^{\times} \quad (5)$$

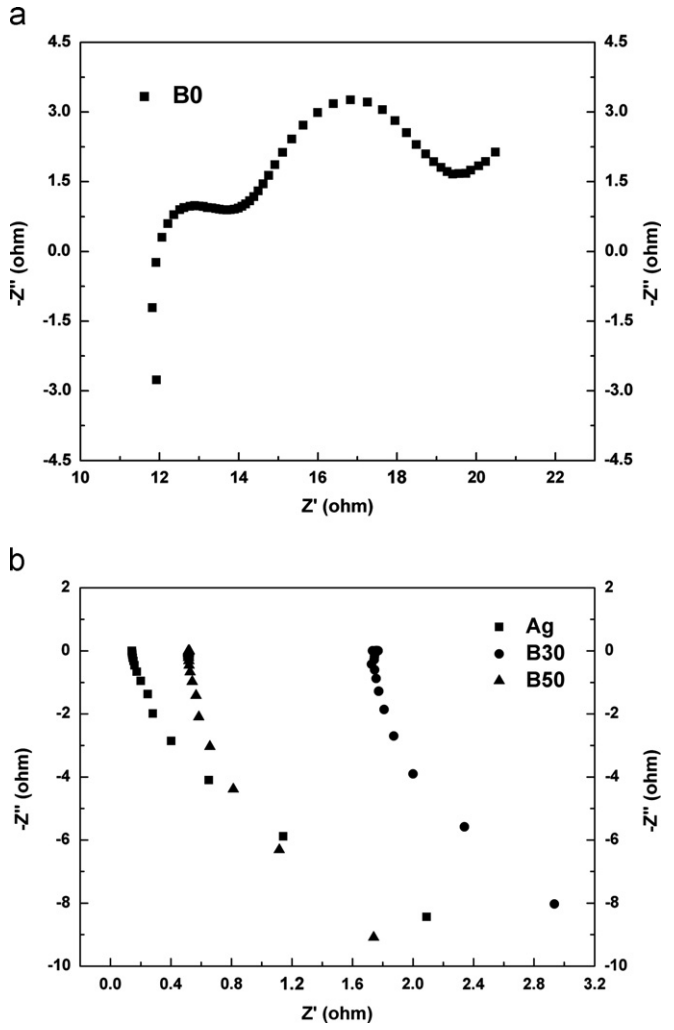

Fig. 7. A.C. impedance spectra of B0, B30, B50 and silver (Ag) thread in wet air at 650 °C.

$$V_O^{\bullet\bullet} + 1/2O_2 \Leftrightarrow O_O^{\times} + 2h^{\bullet} \quad (6)$$

When the atmosphere is humidified, protons come into formation by the following two routes [20]:

$$H_2O + V_O^{\bullet\bullet} \Leftrightarrow 2H^+ + O_O^{\times} \quad (7)$$

$$H_2O + 2h^{\bullet} \Leftrightarrow 2H^+ + 1/2O_2 \quad (8)$$

Hence, the main conductive way for B0 in wet air is through protons and holes (Fig. 8(a)) and protons in wet nitrogen (Fig. 8(b)).

With respect to B30 and B50, firstly, the total conductivities of B30 (0.20 S/cm) and B50 (0.71 S/cm) increase largely with the introduction of Bi, especially for B50. Also, both of them are even one order of magnitude higher than that of B0 (0.019 S/cm) at 700 °C. Secondly, there are some differences in the slope of the Arrhenius curves. The activation energy of the undoped $BaCeO_3$ is ~0.42 eV, which is comparable to the typical value (~0.5 eV, [21,22]) of the protonic conduction in perovskite-type proton conductors. However, the energy for B30 and B50 to realize conduction is up to 0.6–0.7 eV. So based on above

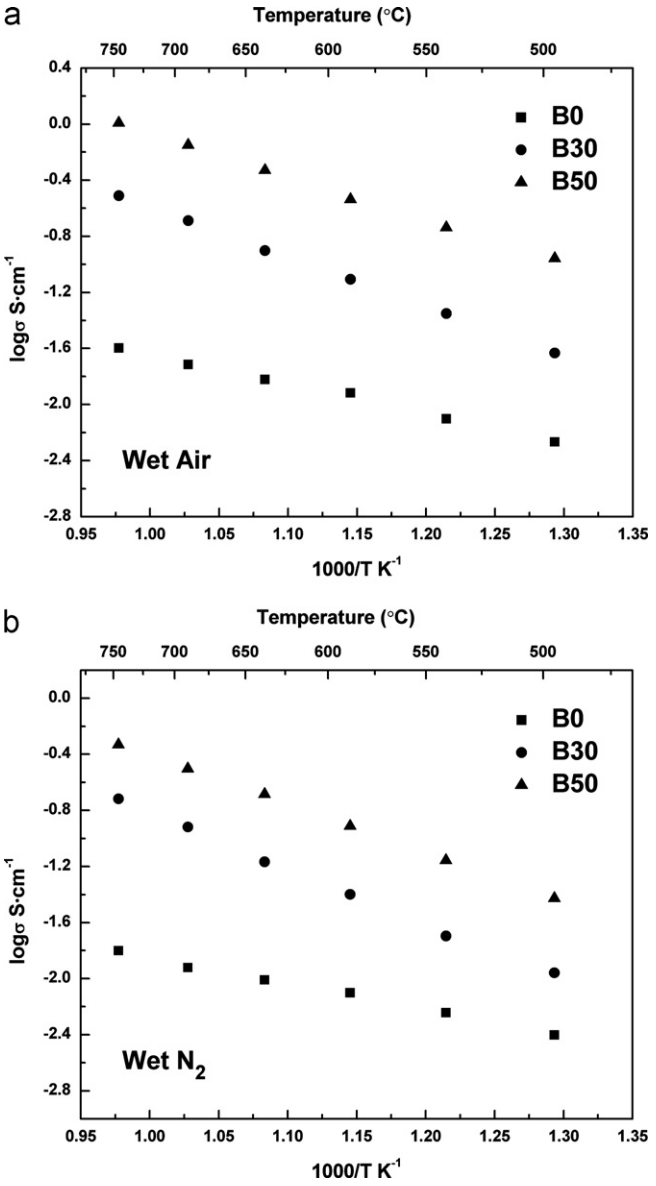

Fig. 8. Arrhenius plots of the total conductivity of B0, B30 and B50 samples under wet air and wet nitrogen.

two aspects, it can be indicated that the mechanism for B30 and B50 is different from that of B0. As mentioned above, both Bi^{3+} and Bi^{5+} ions randomly distribute in B site of the $BaCeO_3$ lattice, which is similar to the most common cathode material—LSM [23–25] with Mn^{2+}, Mn^{3+} and Mn^{4+} ions co-existing in the lattice. The main conductive species in LSM are electrons and one of the conducting ways is that electrons are transported by the Mn ions with different valence states.

Similarly, the transport reaction of electrons in $BaBiO_3$ is

$$Bi_B^{\bullet} \Leftrightarrow Bi_B^{'} + V_O^{\bullet\bullet} \quad (9)$$

Here, B stands for the B sites in ABO_3 perovskite structure. Therefore, unlike B0, a particular conductive way is that electron conduction mainly contributes to the conductivities for B30 and B50 samples. It is of great significance that the

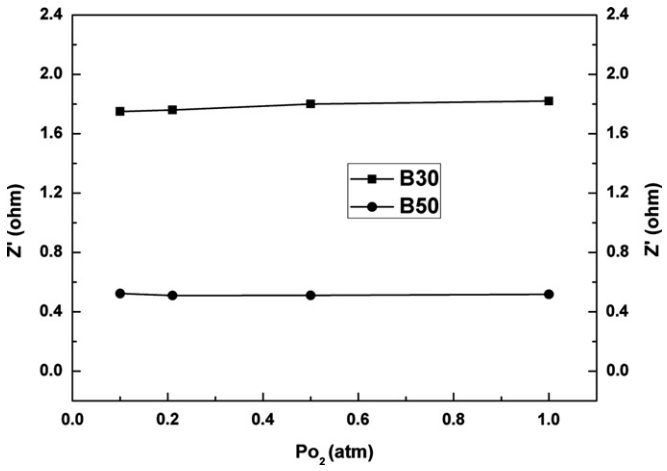

Fig. 9. Change in the total resistance of B30 and B50 samples with the oxygen partial pressure at 650 °C.

assumption is consistent with the previous impedance spectra results (shown in Fig. 7).

When the electrons transport between Bi^{3+} and Bi^{5+} ions, the oxygen vacancies will be occupied according to Eq. (9). It means that the holes formed from the oxygen vacancies are negligible in the system. As a result, the conductivity (or resistance) of the samples containing Bi is irrelevant to the oxygen partial pressure. The total resistance of B30 and B50 samples at 650 °C versus the oxygen partial pressure is shown in Fig. 9. The water vapor partial pressure was kept at the constant value of ~3 kPa. It is evident that all the invariable total resistances with the changes of oxygen partial pressure from 0.1 to 1 atm further verify our assumption that the dominant conductive species in both the Bi-doped samples are electrons.

As shown in Fig. 8(b), the total conductivities of B30 and B50 as a function of temperature in wet nitrogen exhibit similar features to those in wet air. The comparable slopes of both curves indicate the same conductive mechanisms, which are electrons as the main conductive carriers for both doped samples. The conductivity value in wet nitrogen is a little smaller than that in wet air owing to a slightly decreased contribution of electrons resulting from the possible change of some Bi^{5+} ions into Bi^{3+} ions.

4. Conclusion

Pure yttrium and bismuth co-doped $BaCeO_3$ powders were successfully prepared by a citrate–EDTA-based combustion method. Both Bi^{3+} and Bi^{5+} ions were demonstrated to exist in the co-doped $BaCeO_3$ host lattice. The powder sinterability and chemical stability against water vapor were remarkably enhanced with the doping of bismuth, while the tolerance to carbon dioxide was decreased at the same time. The conductivities of B30 and B50 were about one order of magnitude higher than that of the undoped sample at 700 °C in wet air and wet nitrogen owing to the dominant electron conduction between Bi^{3+} and Bi^{5+} ions in both the samples.

Acknowledgments

This work was financially supported by Natural Science Foundation of China (NSFC, Project nos. 50802108 and 51072211) and Science and Technology Commission of Shanghai Municipality (08DZ2210900).

References

[1] H. Iwahara, T. Esaka, H. Uchida, N. Maeda, Proton conduction in sintered oxides and its application to steam electrolysis for hydrogen-production, Solid State Ionics 3-4 (1981) 359–363.
[2] N. Bonanos, K.S. Knight, B. Ellis, Perovskite solid electrolytes: structure, transport properties and fuel cell applications, Solid State Ionics 79 (1995) 161–170.
[3] G. Marnellos, M. Stoukides, Ammonia synthesis at atmospheric pressure, Science 282 (1998) 98–100.
[4] H. Matsumoto, S. Hamajima, T. Yajima, H. Iwahara, Application of hydrogen sensor using proton conductive ceramics as a solid electrolyte to aluminum casting industries, Journal of the Electrochemical Society 148 (2001) D121–D124.
[5] H. Iwahara, High temperature proton conducting oxides and their applications to solid electrolyte fuel cells and steam electrolyzer for hydrogen production, Solid State Ionics 28 (1988) 573–578.
[6] H. Iwahara, H. Uchida, K. Ono, K. Ogaki, Proton conduction in sintered oxides based on $BaCeO_3$, Journal of the Electrochemical Society 135 (1988) 529–533.
[7] K.D. Kreuer, Proton-conducting oxides, Annual Review of Materials Research 33 (2003) 333–359.
[8] K.H. Ryu, S.M. Haile, Chemical stability and proton conductivity of doped $BaCeO_3$–$BaZrO_3$ solid solutions, Solid State Ionics 125 (1999) 355–367.
[9] K. Katahira, Y. Kohchi, T. Shimura, H. Iwahara, Protonic conduction in Zr-substituted $BaCeO_3$, Solid State Ionics 138 (2000) 91–98.
[10] Z.M. Zhong, Stability and conductivity study of the $BaCe_{0.9-x}Zr_xY_{0.1}O_{2.95}$ systems, Solid State Ionics 178 (2007) 213–220.
[11] R.J. Drost, W.T. Fu, Preparation and characterization of the perovskites $BaCe_{1-x}Bi_xO_3$, Materials Research Bulletin 30 (1995) 471–478.
[12] S.H. Lo, C.F. Yang, The sintering characteristics of Bi_2O_3 added MgO–CaO–Al_2O_3–SiO_2 glass powder, Ceramics International 24 (1998) 139–144.
[13] B. Bai, N.M. Sammes, A.L. Smirnova, Physical and electrochemical characterization of Bi_2O_3-doped scandia stabilized zirconia, Journal of Power Sources 176 (2008) 76–81.
[14] D.P. Huang, Q. Xu, W. Chen, H. Wang, R.Z. Yuan, Mixed electronic–ionic conductivity of $La_{0.6}Sr_{0.4}Co_{1-y}Fe_yO_3$ perovskite-type oxides, Journal of Inorganic Materials 20 (2005) 133–138.
[15] J. Azadmanjiri, S.A.Seyyed Ebrahimi, H.K. Salehani, Magnetic properties of nanosize $NiFe_2O_4$ particles synthesized by sol–gel auto-combustion method, Ceramics International 33 (2007) 1623–1625.
[16] Z.M. Wang, Y. Tian, Y.D. Li, Direct CH_4 fuel cell using Sr_2FeMoO_6 as an anode material, Journal of Power Sources 196 (2011) 6104–6109.
[17] K. Xie, R.Q. Yan, X.X. Xu, X.Q. Liu, G.Y. Meng, A stable and thin $BaCe_{0.7}Nb_{0.1}Gd_{0.2}O_{3-\delta}$ membrane prepared by simple all-solid-state process for SOFC, Journal of Power Sources 187 (2009) 403–406.
[18] R.Q. Yan, Q.F. Wang, G.H. Chen, K. Xie, A novel anode-supported stable $BaCe_{0.7}Ta_{0.1}Y_{0.2}O_{3-\delta}$ membrane prepared by all-solid-state process for solid oxide fuel cells, Ionics 15 (2009) 483–486.
[19] S.V. Bhide, A.V. Virkar, Stability of $AB'_{1/2}B''_{1/2}O_3$-type mixed perovskite proton conductors, Journal of the Electrochemical Society 146 (1999) 4386–4392.

[20] H. Uchida, H. Yoshikawa, H. Iwahara, Formation of protons in SrCeO3-based proton conducting oxides. Part 1: Gas evolution and absorption in doped $SrCeO_3$ at high temperature, Solid State Ionics 34 (1989) 103–110.
[21] T. Schober, F. Krug, W. Schilling, Criteria for the application of high temperature proton conductors in SOFCs, Solid State Ionics 97 (1997) 1–4.
[22] A.S. Nowick, A.V. Vaysleyb, Isotope effect and proton hopping in high-temperature protonic conductors, Solid State Ionics 97 (1997) 17–26.
[23] J.A.M. van Roosmalen, E.H.P. Cordfunke, The defect chemistry of $LaMnO_{3\pm\delta}$: 4. Defect model for $LaMnO_{3+\delta}$, Journal of Solid State Chemistry 110 (1994) 109–112.
[24] F.W. Poulsen, Defect chemistry modelling of oxygen-stoichiometry, vacancy concentrations, and conductivity of $(La_{1-x}Sr_x)_yMnO_{3\pm\delta}$, Solid State Ionics 129 (2000) 145–162.
[25] S.P. Jiang, Development of lanthanum strontium manganite perovskite cathode materials of solid oxide fuel cells: a review, Journal of Materials Science 43 (2008) 6799–6833.